Changes in Antigen-Binding Ability of Antibodies Caused by Immobilization on Gold Nanoparticles: A Case Study for Monoclonal Antibodies to Fluorescein

Dmitriy V. Sotnikov [1] , Nadezhda N. Byzova [1], Anatoly V. Zherdev [1], Boris B. Dzantiev [1,*]

[1]   A.N. Bach Institute of Biochemistry, Research Center of Biotechnology of the Russian Academy of Sciences, Moscow, Russia; sotnikov-d-i@mail.ru (D.V.S.); nbyzova@inbi.ras.ru (N.A.B.); zherdev@inbi.ras.ru (A.V.Z.); dzantiev@inbi.ras.ru (B.B.D.);

*   Correspondence: dzantiev@inbi.ras.ru (B.B.D.);

Abstract: Antibody conjugates with gold nanoparticles (GNPs) are widely used in modern diagnostics and theranostics. Therefore, information on these conjugates' composition and functional activity is extremely important. The characterization of antibody complexes with GNPs is typically limited to a qualitative comparison of the concentration dependences for antigen binding. The task of this study was to supplement the existing approaches with quantitative assessments. The number of antibodies absorbed on the surface of GNPs and the percentage of those retaining the antigen-binding ability after immobilization was estimated. The investigation was carried out for 6-carboxyfluorescein as a low molecular weight antigen. Special calculation methods based on the detection of fluorescence of both antibodies and the antigen were proposed. For GNPs with an average diameter of 13 nm, the saturating concentration for antibodies upon monolayer immobilization was established. It was demonstrated that up to 88.8% of antibody binding sites lost their immunochemical activity upon adsorption. Although this value may vary for different antigens, the inactivation factor is significant and should be overcome to obtain highly effective conjugates.

1. Introduction

Antibodies conjugated with gold nanoparticles (GNPs) have been used as analytical probes [1-5] and theranostic reactants [6-8] for many years. The importance of efficient binding and detection of these conjugates causes interest in studying their composition and reactivity [9-11]. However, recent studies demonstrated that immobilization of immunoglobulin molecules on the surface of GNPs could significantly worsen their antigen-binding ability; the difference sometimes reaches an order of magnitude [12-15]. The reasons for such a sharp deterioration remain unclear. This may be because of the inefficient orientation of immobilized molecules, steric or electrostatic limitations for contact with an antigen, and other factors postulated in various studies [16-19]. However, the contribution of these factors was not compared.

Existing publications are limited to the comparison of free and bound antibodies. However, the antibodies are not guaranteed full functionality before their conjugation. It is known that antibodies undergo significant structural changes during storage up to their partial

disintegration into fragments [20, 21]. The inactivation of immunoglobulins in solutions depends on many factors related to the medium composition and storage conditions [20, 22, 23] and the immunoglobulins' structure [24-26]. Even mechanical actions such as shaking or mixing can significantly influence the state of immunoglobulins [27].

In this investigation, the antigen-binding ability of antibodies (both free and adsorbed on the surface of GNPs) was studied using 6-carboxyfluorescein (FAM) as an antigen and anti-FAM monoclonal antibodies (mAbs). The strong fluorescence of the chosen antigen allows for determining its concentration in solution with high accuracy. The binding of FAM with specific mAbs almost completely suppresses its fluorescence [28, 29]. Due to this, the antigen-antibody complex formation can be detected in real-time conditions without additional stages of isolation or treatment by extra reagents. These reasons make the chosen pair a very perspective model system to study the influence of GNPs on the properties of mAbs adsorbed on their surface.

2. Materials and Methods

2.1. Materials.

MAbs against fluorescein from HyTest (Moscow, Russia) were used. FAM, gold (III) chloride hydrate ($HAuCl_4$), Tris, and sodium citrate were purchased from Sigma-Aldrich (St. Louis, MO, USA). Monofunctional poly(ethylene glycol) with reactive free thiol groups (MPEG-SH; m.w. 5 kDa) was purchased from Creative PEGWorks (Durham, NC, USA). All other reagents were purchased from Khimmed (Moscow, Russia). Deionized water produced by Milli-Q (Millipore; Burlington, MA, USA) was used to prepare solutions.

2.2. Obtaining and characterization of GNPs.

Spherical GNPs with an average diameter of 13 nm were synthesized by the citrate method of Turkevich-Frens [30]. For this, $HAuCl_4$ (1 mL of 1% solution) was added to deionized water (96.5 mL) and brought to boiling. Then, sodium citrate (2.5 mL of 1% solution) was added under stirring. After 15-min incubation, the mixture was cooled to room temperature and stored at 4°C.

To perform transmission electron microscopy (TEM), GNPs were applied to grids (300 mesh) covered by a film of polyvinyl formal dissolved in chloroform. TEM images were obtained on a JEM CX-100 electron microscope (Jeol, Tokyo, Japan) at an accelerating voltage of 80 kV and a magnification of 3,300,000. The digital microphotographs were analyzed using Image Tool software (University of Texas Health Science Center, San Antonio, TX, USA). The absorption spectra of GNPs were registered on a Libra S80 spectrophotometer (Biochrom, Cambridge, UK) in the wavelength range of 400–700 nm.

2.3. Conjugation of GNPs with mAbs.

Initially, mAbs were dialyzed against 1,000-fold excess of 10 mM Tris-HCl buffer, pH 9.0, for 2 h at 4–6°C. Potassium carbonate solution (0.1 M) was added to the GNPs solution (optical density at 520 nm (OD_{520}) = 1.0) until pH 9.0 was reached. After this, GNPs were added to mAbs and incubated for 30 min at room temperature with stirring. Then, an aqueous solution of PEG-SH was added to a final concentration of 0.25%. The obtained mAb–GNP conjugates were twice centrifuged on an Allegra 64R centrifuge (Beckman Coulter, Brea, CA,

USA) at 25,000 g and 4°C for 15 min. The supernatants and the pellets were collected. The latter containing GNP–mAb conjugates were diluted with 50 mM phosphate buffer, pH 7.4, containing 0.1 M NaCl (PBS) with 0.25% PEG-SH to OD_{520} = 5.0.

2.4. Determination of mAbs binding capacity.

2.4.1. Method 1.

Wells of a white microplate (Nunc MaxiSorp, Roskilde, Denmark) were filled with PBS (100 µL). A FAM solution (2 µg/mL, 100 µL) was added to the first row of wells. Then, a series of FAM dilutions were obtained by a sequential transfer of its solutions (100 µL) to the next rows. Then, mAbs (15 µg/mL, 100 µL) were added to half of the microplate and PBS (100 µL) – to the other half. The mixtures were incubated for 10 min at room temperature, and the fluorescence was measured (see Section 2.7). Signal values registered for antibody-free solutions were used to construct a calibration curve. Signal values for solutions containing both FAM and mAbs were used to calculate the amount of the bound antigen based on the difference in fluorescence measured in the calibration solutions.

2.4.2. Method 2.

Wells of a white microplate were filled with PBS (100 µL). A solution of mAbs (150 µg/mL, 100 µL) was added to the first row of wells. Then, a series of mAbs dilutions were obtained by a sequential transfer of their solutions (100 µL) to the next rows. Then a FAM solution (100 ng/mL, 100 µL) was added to the wells and incubated for 10 min at room temperature. After fluorescence measurements, the amount of the bound and free antigen was calculated (see Results and Discussion).

2.5. Determination of the amount of mAbs bound to GNPs.

The composition of the mAb–GNP conjugate was determined using the earlier developed protocol [15, 31]. The supernatants obtained after the centrifugation were divided into 2 equal parts. MAbs were added to the first part (to reach the final concentration of 3.15 µg/mL) to obtain calibration solutions; nothing was added to the second part. The resulting solutions were poured into 96-well microplates (200 µL per well, 2 repetitions for each solution), and the fluorescence was measured. The difference in fluorescence for solutions containing mAbs and without them corresponds to the fluorescence of mAbs at a concentration of 3.15 µg/mL. This value was used to calculate the concentration of mAbs in the supernatant (µg/mL) by the formula:

$$F \times C / (Fc - F) \tag{1}$$

where F is the fluorescence of the supernatant, Fc is the fluorescence of the supernatant with the added mAbs, and C is the concentration of the added mAbs (3.15 µg/mL).

The difference between the concentration mAbs added to the reaction solution, and the concentration of mAbs in the supernatant corresponds to the mAbs content in the corresponding conjugate with GNPs.

2.6. Determination of the amount of active mAbs on the GNP surface.

Mab–GNP conjugates (OD_{520} = 5.0) were divided into 7 parts of 1.5 mL each. FAM solutions were added to 6 parts to reach 2–125 ng/mL final concentrations. The seventh part

contained no FAM. The mixtures were incubated for 30 min at room temperature with stirring and then centrifuged twice at the aforementioned regime. The supernatants were collected to determine bound and unbound antigens in the same way as it was described above for bound and unbound mAbs.

2.7. Fluorescence measurement.

Fluorescence spectra were recorded in white microplates using a Perkin Elmer EnSpire 2300 microplate reader (Waltham, MA, USA). For mAbs and FAM, the excitation wavelength/the emission wavelength ranges were 280/290–500 nm and 502/522–600 nm, respectively.

3. Results and Discussion

3.1. Study of fluorescence quenching of FAM by mAbs.

The strong influence of the nearest environment of a fluorophore on its fluorescence is well known [32-34]. It can be manifested either in the complete quenching of the fluorescence or its amplification. The quenching of FAM fluorescence in its complexes with mAbs was observed in our previous experiments [29]. Figure 1 demonstrates the fluorescence spectra of FAM in PBS and mixtures with excessive concentrations of mAbs. According to the obtained data, the fluorescence is almost completely quenched (>96%). For each solution, the spectra were recorded twice at 10-min intervals. The first and the second measurements completely coincided, which indicated equilibrium reaching.
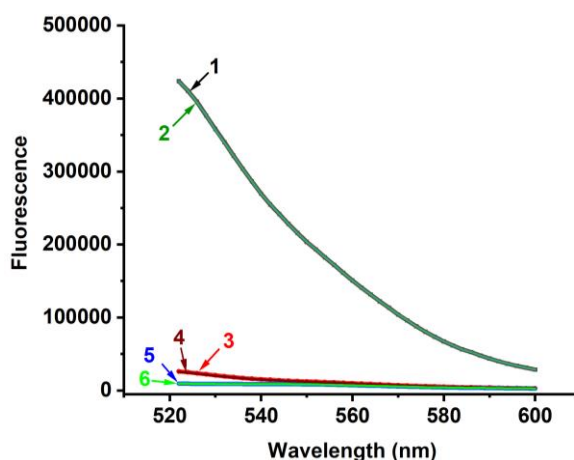
Figure. 1. Fluorescence spectra of FAM and FAM –mAb complex. 1. – FAM 100 ng/mL; 2. – FAM 100 ng/mL after 10 min; 3. – FAM 100 ng/mL + mAbs 75 µg/mL; 4. – FAM 100 ng/mL + mAbs 75 µg/mL after 10 min; 5. – PBS; 6. –PBS after 10 min.

3.2. Interaction of FAM with mAbs.

The effect of quenching was applied to register the binding of FAM with mAbs in the solution. Two methods were used to improve reliability.

3.2.1. Method 1.

Two rows of FAM solutions with concentrations of 0.4–500 ng/mL were prepared. The first row also contained mAbs (7.5 µg/mL). The second row without mAbs was used for calibration. According to Figure 2a, the calibration dependence was almost linear up to FAM

concentrations of about 60 ng/mL. The dependence of the fluorescence on the fluorophore concentration for solutions containing mAbs (Figure 2b) was more complex. At FAM concentrations of less than 15 ng/mL, the fluorescence was almost completely quenched by the excess of mAbs and practically did not differ from the background. With an increase in the FAM concentration, the binding centers of mAbs became occupied, and the concentration of free FAM grew, which was accompanied by the fluorescence increase. The point separating these regions accorded to the equimolar antigen/antibody ratio (Figure 2b).

| (a) | (b) |
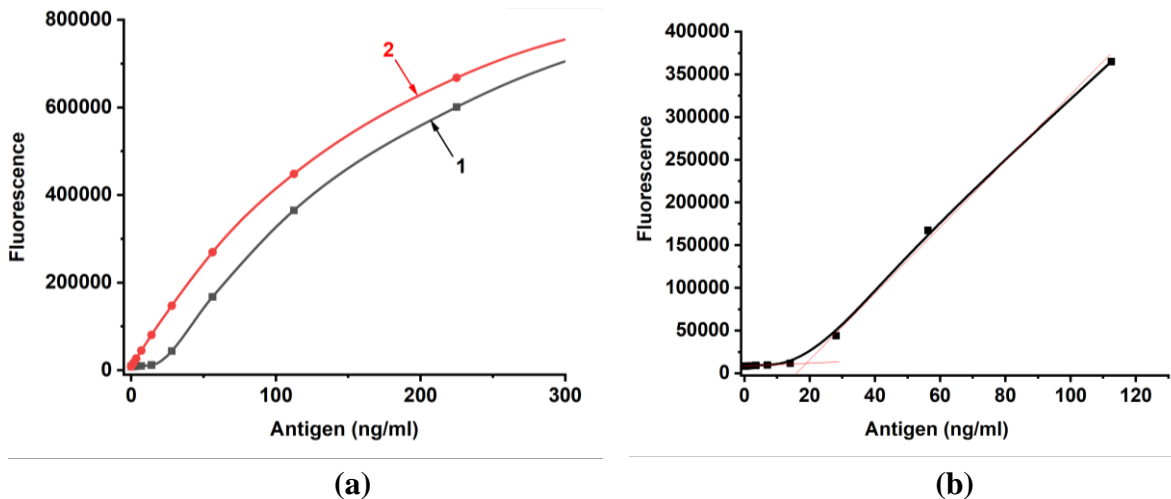
Figure 2. Fluorescence at 522 nm of (**a**) 1. – mixtures of different concentrations of FAM with 7.5 µg/mL of antibodies and 2. – FAM calibration solutions; (**b**) the initial section of the curve (a).
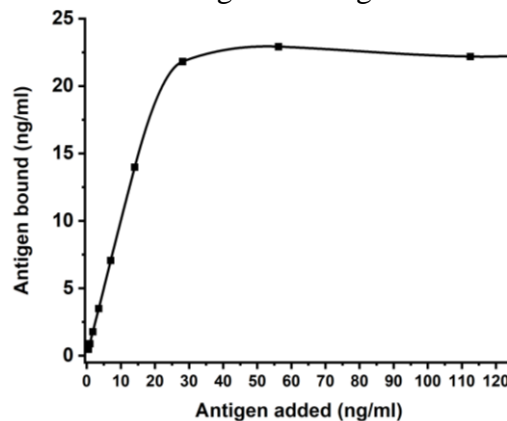
The free and antibody-bound FAM concentrations were calculated based on the obtained data using the following reasoning. The total fluorescence minus the background (F) is the sum of the fluorescence of free and bound FAM. The maximum fluorescence is observed at 522 nm. At a given wavelength, the fluorescence of bound FAM is 4% of the fluorescence of free FAM in the same concentration (Figure 1). The fluorescence is also equal to the fluorescence of the unit concentration of the fluorophore (F_1) multiplied by its concentration. Therefore:

$$F = F_1 \times C_f + 0.04 \times F_1 \cdot \times C_b, \tag{2}$$

where C_f and C_b are the concentrations of free and bound FAM, respectively. Considering that $C_f + C_b$ is the total added concentration of FAM:

$$C_f = (F / F_1 - 0.04 \times C) / 0.96 \tag{3}$$

The dependence of the concentration of bound FAM on its initially added concentration (Figure 3) showed saturation of mAbs' antigen-binding sites.

Figure 3. Dependence of antibody-bound FAM concentration on the total FAM concentration in the solution.

Based on these results and the known concentration of bivalent mAbs (immunoglobulins of G class, IgG), the percentage of active antigen-binding centers was calculated. The calculation was performed for three FAM concentrations: 112.5, 56.3, and 28.1 ng/mL. At lower concentrations, the saturation of all active sites of mAbs was not achieved, whereas higher concentrations deviated from a linear dependence increasing the measurement error. According to the obtained results (Table 1), 58–61% of the antigen-binding centers retained their ability to bind FAM.

Table 1. Concentrations of the total, free, and antibody-bound FAM and the percentage of mAbs' active valences.

FAM concentration, ng/mL (nM)	Fluorescence at 522 nm	Concentration of bound FAM, nM	Concentration of free FAM, nM	Active antibody valence (%)
112.5 (299.2)	356485	59.0	240.2	59
56.3 (149.6)	158927	61.0	88.6	61
28.1 (74.8)	35464	58.0	16.8	58

3.2.2. Method 2.

According to the second method, mAbs at concentrations of 0.04–37.5 µg/mL were added to the solution of FAM at a fixed concentration (50 ng/mL). After 10-min incubation, the fluorescence was measured. The observed dependence of fluorescence on mAbs concentrations was characterized by the region of mAbs excess (where the fluorescence was almost completely quenched) and that of FAM excess (where the fluorescence increased with a decrease in mAbs concentration) (Figure 4). The intersection of these regions roughly corresponded to the equivalence zone. For an accurate calculation of active antigen-binding sites, the mAbs excess region is unsuitable because the fluorescence is completely quenched. It should be noted that the lower the concentration of mAbs, the smaller the difference between the fluorescence of the solution and at zero point (without mAbs), and the higher the error. For mAbs concentrations less than 1 µg/mL, errors exceed the fluorescence difference at the adjacent points. Therefore, these values were not used for calculations.
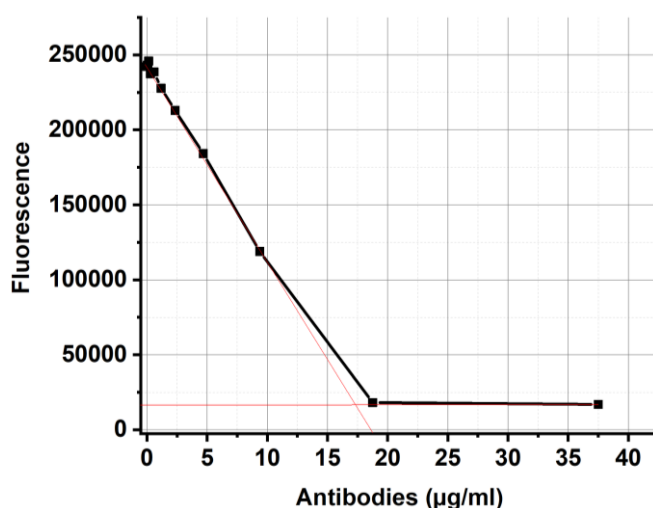
Figure 4. Dependence of the fluorescence (at 522 nm) of mAbs-containing FAM solutions on mAbs concentrations.

For the remaining four concentrations of mAbs, the concentrations of antigen-binding sites were calculated using formula (2), taking into account the bivalence of IgG. According to the data obtained (Table 2), 55–59% of the antigen-binding sites of mAbs in solution retained

their binding ability. We consider that 59% is a more reliable value because here, the fluorescence has the greatest difference from the zero point, and the influence of the measurement errors is minimal. According to the results of the two methods, the activity of mAbs was 55–61% (the mean value is 58%).

Table 2. Concentrations of mAbs and antibody-bound FAM.

Concentration of mAbs, µg/mL (nM)	Concentration of antigen-binding sites, nM	Fluorescence at 522 nm	Concentration of bound FAM, nM	Active valences (%)
9.4 (62.5)	125	109520	73.4	59
4.7 (31.3)	62.5	174712	34.6	55
2.3 (15.6)	31.3	203584	17.4	56
1.2 (7.8)	15.6	218351	8.61	55

3.3. Characterization of GNPs.

The size and homogeneity of GNPs used in the study were controlled using TEM, as described earlier [35]. According to the data obtained, the average diameter of GNPs was 13 ± 2 nm. The synthesized GNPs were also characterized spectrophotometrically. Generally, GNPs have a typical absorption peak at 515–540 nm, which is associated with surface plasmon resonance (the resonance between the frequency of collective oscillations of free electrons on the GNP surface and the frequency of the light wave) [36]. The synthesized GNPs had an absorption maximum of 517.5 nm. According to the dependence between the GNP size and the absorption maximum described in [15], it corresponded to GNPs with the given diameter.

3.4. Obtaining mAb-GNP conjugates and determination of their composition.

The synthesized GNPs were mixed with mAbs to their final concentration of 13.4 µg/mL. This concentration was selected so that one IgG molecule would occupy 25 nm^2 of the GNP surface area. Taking into account the dimensions of the IgG molecule, this concentration ensured a formation of a monolayer of mAbs [31]. The calculated concentration of GNPs in the solution was 22.2×10^{12} particles/mL.

The number of IgG molecules adsorbed on a GNP was determined using the technique proposed in our previous studies [15, 31]. This method is based on measuring the fluorescence of tryptophan residues in IgG molecules. The amount of bound antibodies is calculated by comparing the initial fluorescence of the calibration solutions (F_0) and the residual fluorescence of the reaction solutions after separating the synthesized conjugates by centrifugation (F). The difference between these two values (ΔF) corresponds to the content of protein in the conjugate:
$$C_k = C_0 \cdot \times \Delta F / F_0, \qquad (4)$$
where C_0 is the concentration of the added protein and C_k is the protein concentration in the conjugate solution. Based on the measured fluorescence values, 12.9 µg/mL of mAbs were bound to the GNPs. Taking into account that the concentration of the added mAbs was 13.4 µg/mL, almost all the added antibodies become adsorbed on GNPs.

3.5. Study of the antigen-binding ability of mAbs conjugated with GNPs.

Similar to free mAbs, conjugated antibodies also suppress the fluorescence of FAM. However, because the solution of GNPs is colored, the fluorescence value is affected by the interaction with mAbs and the GNP-based reabsorption of FAM fluorescence. As a result, when mAb–GNP conjugate is added to the FAM solution, the fluorescence decreases by more

than an order of magnitude, even for excess concentrations of FAM. To determine the quenching of FAM by mAbs, two stages of antigen addition were considered. At the first stage, FAM was added to the mAb–GNP conjugate (OD_{520} = 1.6) to final concentrations of 2–125 ng/mL, and then, the fluorescence was measured. As in the case of unlabeled antibodies, the obtained dependence demonstrates a region with completely suppressed fluorescence (at the excess of mAbs) and a region of linear fluorescence growth with increasing antigen concentration (at the excess of FAM) (Figure 5).

Additional FAM portions were added to solutions containing excessive FAM concentrations to obtain a final FAM concentration of 7.5 ng/mL. These FAM portions do not bind with mAbs. Therefore, the difference in fluorescence before and after the addition corresponds to the fluorescence of the added FAM. This value can be used for the calibration because the reabsorption by GNPs is the same for both series of solutions. Based on the resulting dependencies (Figure 5), the concentration of free FAM (C, ng/mL) in each sample was calculated using the formula:

$$C = F \times 7.5 / (F_c - F) \tag{5}$$

where F is the sample's fluorescence, F_c is the fluorescence of calibration solutions, and 7.5 is the concentration of an additional portion of FAM (ng/mL).
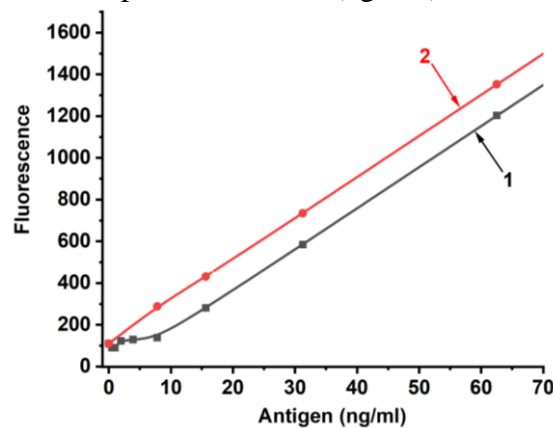
Figure 5. 1. – Dependence of fluorescence at 522 nm for FAM solutions with GNP-antibody conjugates on the concentration of the added antigen; 2. – Calibration curve.

By subtracting the calculated concentration of free FAM from the initial concentration of FAM, the concentration of FAM bound to GNP-labeled mAbs can be obtained. The dependence of the bound FAM on the initially added one demonstrates the saturation of antigen-binding sites of the labeled mAbs upon increasing the FAM concentration (Figure 6). The maximum concentration of the bound FAM was 7.9 ng/mL (21 nM).
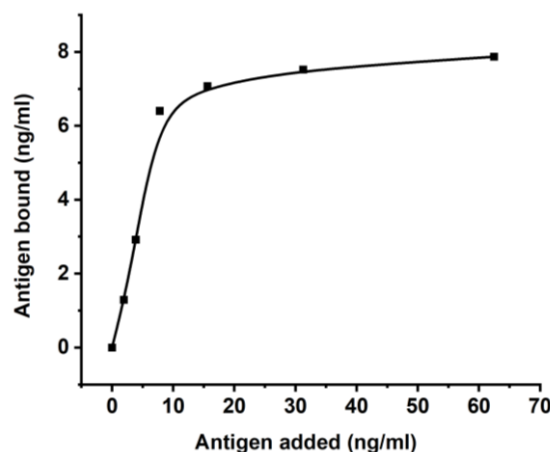
Figure. 6. Binding of FAM to mAb-GNP conjugates with increasing concentration of the added FAM.

Overall, 12.9 µg/mL (85.9 nM) of mAbs were bound to GNPs. After centrifugation, the conjugate was concentrated 5.8 times, and after mixing with FAM, it was diluted 3.2 times. Thus, after all manipulations, the conjugate was concentrated 1.8 times and contained 155.7 nM of mAbs. Taking into account the IgG bivalence, 311.4 nM of antigen-binding centers was obtained, which bound 21 nM of FAM. This means that after conjugation with GNPs, only 6.7% of the antigen-binding sites remain active. Given that about 60% of the antigen-binding centers in the original mAbs preparation are active, only 11.2% retained their binding capacity after conjugation, i.e., the inactivation degree was 88.8%.

4. Conclusions

The obtained results demonstrate a significant loss of antigen-binding activity by mAbs upon adsorption on the surface of GNPs. Although the present case study covers a single antigen, which individual properties may contribute to the inactivation, the discussed problem still has a general character. Thus, in studies with protein antigens, the residual binding capacity of immobilized antibodies was approximately 17-34% [12-15]. Furthermore, our data demonstrate that in the case of low molecular weight antigens, for which steric obstacles to the occupation of all binding sites are excluded, the residual antigen-binding activity of antibodies can be even lower. Therefore, to ensure the high efficiency of antibody-nanoparticle complexes, standard protocols for mAbs immobilization at concentrations selected based on the flocculation curve or calculated monolayer [37-40] require improvements. In this regard, approaches based on the increased reactivity of the obtained conjugates are promising. They include oriented covalent immobilization with the modification of gold surface [41-43], the use of immunoglobulin-binding proteins [44, 45], and the optimal non-saturating loading of antibodies on the surface of nanoparticles [46, 47].

Funding

Conflicts of Interest

The authors declare no conflict of interest.

References

1. Lee, J.W.; Choi, S.R.; Heo, J.H. Simultaneous stabilization and functionalization of gold nanoparticles via biomolecule conjugation: Progress and perspectives. *ACS Appl. Mater. Interfaces* **2021**, *13*, 42311-42328, https://doi.org/10.1021/acsami.1c10436.
2. Lin, X.; O'Reilly Beringhs, A.; Lu, X. Applications of nanoparticle-antibody conjugates in immunoassays and tumor imaging. *The AAPS J.* **2021**, *23*, 43, https://doi.org/10.1208/s12248-021-00561-5.
3. Wu, L.; Wang, M.; Wei, D. Advances in gold nanoparticles for mycotoxin analysis. *Analyst* **2021**, *146*, 1793-1806, https://doi.org/10.1039/D0AN02171G.
4. Marin, M.; Nikolic, M.V.; Vidic, J. Rapid point-of-need detection of bacteria and their toxins in food using gold nanoparticles. *Compr. Rev. Food Sci. Food Saf.* **2021**, *20*, 5880-5900, https://doi.org/10.1111/1541-4337.12839.
5. Tabatabaei, M.S.; Islam, R.; Ahmed, M. Applications of gold nanoparticles in ELISA, PCR, and immuno-PCR assays: a review. *Anal. Chim. Acta* **2021**, *1143*, 250-266, https://doi.org/10.1016/j.aca.2020.08.030.

6. Niloy, M.S.; Shakil, M.; Hossen, M.; Alam, M.; Rosengren, R.J. Promise of gold nanomaterials as a lung cancer theranostic agent: a systematic review. *Int. Nano Lett.* **2021**, *11*, 93–111, https://doi.org/10.1007/s40089-021-00332-2.

7. Medici, S.; Peana, M.; Coradduzza, D.; Zoroddu, M.A. Gold nanoparticles and cancer: Detection, diagnosis and therapy. *Semin. Cancer Biol.* **2021**, *76*, 27-37, https://doi.org/10.1016/j.semcancer.2021.06.017.

8. Shete, M.B.; Patil, T.S.; Deshpande, A.S.; Saraogi, G.; Vasdev, N.; Deshpande, M.; Rajpoot, K.; Tekade, R.K. Current trends in theranostic nanomedicines. *J. Drug Deliv. Sci. Technol.* **2022**, *71*, 103280, https://doi.org/10.1016/j.jddst.2022.103280.

9. Zhang, L.; Mazouzi, Y.; Salmain, M.; Liedberg, B.; Boujday, S. Antibody-gold nanoparticle bioconjugates for biosensors: synthesis, characterization and selected applications. *Biosens. Bioelectron.* **2020**, *165*, 112370, https://doi.org/10.1016/j.bios.2020.112370.

10. Busch, R.T.; Karim, F.; Weis, J.; Sun, Y.; Zhao, C.; Vasquez, E.S. Optimization and structural stability of gold nanoparticle–antibody bioconjugates. *ACS Omega* **2019**, *4*, 15269-15279, https://doi.org/10.1021/acsomega.9b02276.

11. Safenkova, I.V.; Zherdev, A.V.; Dzantiev, B.B. Correlation between the composition of multivalent antibody conjugates with colloidal gold nanoparticles and their affinity. *J. Immunol. Methods* **2010**, *357*, 17-25, https://doi.org/10.1016/j.jim.2010.03.010.

12. Sotnikov, D.V.; Radchenko, A.S.; Zherdev, A.V.; Dzantiev, B.B. Determination of the composition and functional activity of the conjugates of colloidal gold and antibodies. *Eurasian J. Anal. Chem.* **2016**, *11*, 169-179, https://doi.org/10.12973/ejac.2016.130a.

13. Tripathi, K.; Driskell, J.D. Quantifying bound and active antibodies conjugated to gold nanoparticles: a comprehensive and robust approach to evaluate immobilization chemistry. *ACS Omega* **2018**, *3*, 8253-8259, https://doi.org/10.1021/acsomega.8b00591.

14. Ruiz, G.; Tripathi, K.; Okyem, S.; Driskell, J. D. pH impacts the orientation of antibody adsorbed onto gold nanoparticles. *Bioconjug. Chem.* **2019**, *30*, 1182-1191, https://doi.org/10.1021/acs.bioconjchem.9b00123.

15. Sotnikov, D.V.; Byzova, N.A.; Zherdev, A.V.; Dzantiev, B.B. Retention of activity by antibodies immobilized on gold nanoparticles of different sizes: Fluorometric method of determination and comparative evaluation. *Nanomater.* **2021**, *11*, 3117, https://doi.org/10.3390/nano11113117.

16. Parolo, C.; Sena-Torralba, A.; Bergua, J.F.; Calucho, E.; Fuentes-Chust, C.; Hu, L.; Rivas, L.; Alvarez-Diduk, R.; Nguyen, E.P.; Cinti, S.; Quesada-González, D.; Merkoci, A. Tutorial: Design and fabrication of nanoparticle-based lateral-flow immunoassays. *Nat. Protoc.* **2020**, *15*, 3788–3816, https://doi.org/10.1038/s41596-020-0357-x.

17. Lou, D.; Ji, L.; Fan, L.; Ji, Y.; Gu, N.; Zhang, Y. Antibody-oriented strategy and mechanism for the preparation of fluorescent nanoprobes for fast and sensitive immunodetection. *Langmuir* **2019**, *35*, 4860-4867, https://doi.org/10.1021/acs.langmuir.9b00150.

18. Sotnikov, D.V.; Berlina, A.N.; Ivanov, V.S.; Zherdev, A.V.; Dzantiev, B.B. Adsorption of proteins on gold nanoparticles: One or more layers? *Colloids Surf. B: Biointerfaces* **2019**, *173*, 557-563, https://doi.org/10.1016/j.colsurfb.2018.10.025.

19. Goossens, J.; Sein, H.; Lu, S.; Radwanska, M.; Muyldermans, S.; Sterckx, Y.G.J.; Magez, S. Functionalization of gold nanoparticles with nanobodies through physical adsorption. *Anal. Methods* **2017**, *9*, 3430-3440, https://doi.org/10.1039/C7AY00854F.

20. Gaza-Bulseco, G.; Liu, H. Fragmentation of a recombinant monoclonal antibody at various pH. *Pharm. Res.* **2008**, *25*, 1881-1890, https://doi.org/10.1007/s11095-008-9606-3.

21. Vlasak, J.; Ionescu, R. Fragmentation of monoclonal antibodies. *MAbs* **2011**, *3*, 253-263, https://doi.org/10.4161/mabs.3.3.15608.

22. Ferraz, A.S.; Belo, E.F.; Coutinho, L.M.; Oliveira, A.P.; Carmo, A.; Franco, D.L.; Ferreira, T.; Yto, A.Y.; Machado, M.S.; Scola, M.C.; De Gaspari, E. Storage and stability of IgG and IgM monoclonal antibodies dried on filter paper and utility in *Neisseria meningitidis* serotyping by dot-blot ELISA. *BMC Infect. Dis.* **2008**, *8*, 30, https://doi.org/10.1186/1471-2334-8-30.

23. Gupta, S.; Jiskoot, W.; Schöneich, C.; Rathore, A.S. Oxidation and deamidation of monoclonal antibody products: potential impact on stability, biological activity, and efficacy. *J. Pharm. Sci.* **2021**, *111*, 903-918, https://doi.org/10.1016/j.xphs.2021.11.024.

24. Liu, H.; Nowak, C.; Andrien, B.; Shao, M.; Ponniah, G.; Neill, A. Impact of IgG Fc oligosaccharides on recombinant monoclonal antibody structure, stability, safety, and efficacy. *Biotechnol. Prog.* **2017**, *33*, 1173-1181, https://doi.org/10.1002/btpr.2498.

25. Correia, I. Stability of IgG isotypes in serum. *MAbs* **2010**, *2*, 221-232, https://doi.org/10.4161/mabs.2.3.11788.

26. Liu, H.; May, K. Disulfide bond structures of IgG molecules: structural variations, chemical modifications and possible impacts to stability and biological function. *MAbs* **2012**, *4*, 17-23, https://doi.org/10.4161/mabs.4.1.18347.

27. Kiese, S.; Papppenberger, A.; Friess, W.; Mahler, H.C. Shaken, not stirred: Mechanical stress testing of an IgG1 antibody. *J. Pharm. Sci.* **2008**, *97*, 4347-4366, https://doi.org/10.1002/jps.21328.

28. Watt, R.M.; Voss Jr, E.W. Mechanism of quenching of fluorescein by anti-fluorescein IgG antibodies. *Immunochemistry* **1977**, *14*, 533-541, https://doi.org/10.1016/0019-2791(77)90308-1.

29. Ivanov, A.V.; Safenkova, I.V.; Zherdev, A.V.; Dzantiev, B.B. DIRECT²: A novel platform for a CRISPR–Cas12-based assay comprising universal DNA–IgG probe and a direct lateral flow test. *Biosens. Bioelectron.* **2022**, *208*, 114227, https://doi.org/10.1016/j.bios.2022.114227.

30. Frens, G. Controlled nucleation for the regulation of the particle size in monodisperse gold suspensions. *Nature* **1973**, *241*, 20-22, https://doi.org/10.1038/physci241020a0.

31. Sotnikov, D.V.; Zherdev, A.V.; Dzantiev, B.B. Development and application of a label-free fluorescence method for determining the composition of gold nanoparticle–protein conjugates. *Int. J. Mol. Sci.* **2015**, *16*, 907-923, https://doi.org/10.3390/ijms16010907.

32. Zacharioudaki, D.E.; Fitilis, I.; Kotti, M. Review of fluorescence spectroscopy in environmental quality applications. *Molecules* **2022**, 27, 4801, https://doi.org/10.3390/molecules27154801.

33. Patil, U.; Goyal, A.; Vu, B.; Liu, Y.; Maranholkar, V.; Kourentzi, K.; Briggs J.M., Willson, R.C. Antibody mix-and-read assays based on fluorescence intensity probes. *MAbs* **2021**, *13*, 1980178, https://doi.org/10.1080/19420862.2021.1980178.

34. Kang, K.; Wang, J.; Jasinski, J.; Achilefu, J. Fluorescent manipulation by gold nanoparticles: From complete quenching to extensive enhancement. *J. Nanobiotechnol.* **2011**, *9*, 16, https://doi.org/10.1186/1477-3155-9-16.

35. Byzova, N.A.; Zherdev, A.V.; Pridvorova, S.M.; Dzantiev, B.B. Development of rapid immunochromatographic assay for D-dimer detection. *Appl. Biochem. Microbiol.* **2019**, *55*, 305-312, https://doi.org/10.1134/S0003683819030062.

36. Man, S.-Q.; Guo, J.; Liu, Y. Calculation extinction cross sections and molar attenuation coefficient of small gold nanoparticles and experimental observation of their UV–vis spectral properties. *Spectrochim. Acta A: Mol. Biomol. Spectrosc.* **2018**, *191*, 513-520, https://doi.org/10.1016/j.saa.2017.10.047.

37. Geoghegan, W.D.; Ackerman, G.A. Adsorption of horseradish peroxidase, ovomucoid and anti-immunoglobulin to colloidal gold for the indirect detection of concanavalin A, wheat germ agglutinin and goat anti-human immunoglobulin G on cell surfaces at the electron microscopic level: a new method, theory and application. *J. Histochem. Cytochem.* **1977**, *25*, 1187-1200, https://doi.org/10.1177/25.11.21217.

38. Horisberger, M.; Rosset, J. Colloidal gold, a useful marker for transmission and scanning electron microscopy. *J. Histochem. Cytochem.* **1977**, *25*, 295-305, https://doi.org/10.1177/25.4.323352.

39. Pamies, R.; Cifre, J.G.H.; Espín, V.F.; Collado-González, M.; Baños, F.G.D.; de la Torre, J.G. Aggregation behaviour of gold nanoparticles in saline aqueous media. *J. Nanoparticle Res.* **2014**, *16*, 2376, https://doi.org/10.1007/s11051-014-2376-4.

40. Seiler, L.K.; Jonczyk, R.; Lindner, P.; Phung, N.L.; Falk, C.S.; Kaufeld, J.; Gwinner, W.; Scheffner, I.; Immenschuh, S.; Blume, C. A new lateral flow assay to detect sIL-2R during T-cell mediated rejection after kidney transplantation. *Analyst* **2021**, *146*, 5369-5379, https://doi.org/10.1039/D1AN01001H.

41. Jazayeri, M.H.; Amani, H.; Pourfatollah, A.A.; Pazoki-Toroudi, H.; Sedighimoghaddam, B. Various methods of gold nanoparticles (GNPs) conjugation to antibodies. *Sens. Bio-Sens. Res.* **2016**, *9*, 17-22, https://doi.org/10.1016/j.sbsr.2016.04.002.

42. Zhou, S.; Hu, J.; Chen, X.; Duan, H.; Shao, Y.; Lin, T.; Li X.; Huang, X.; Xiong, Y. Hydrazide-assisted directional antibody conjugation of gold nanoparticles to enhance immunochromatographic assay. *Anal. Chim. Acta* **2021**, *1168*, 338623, https://doi.org/10.1016/j.aca.2021.338623.

43. Oliveira, J.P.; Prado, A.R.; Keijok, W.J.; Antunes, P.W.P., Yapuchura, E.R., Guimarães, M.C.C. Impact of conjugation strategies for targeting of antibodies in gold nanoparticles for ultrasensitive detection of 17β-estradiol. *Sci. Rep.* **2019**, *9*, 13859, https://doi.org/10.1038/s41598-019-50424-5.

44. von Witting, E.; Hober, S.; Kanje, S. Affinity-based methods for site-specific conjugation of antibodies. *Bioconjug. Chem.* **2021**, *32*, 1515-1524, https://doi.org/10.1021/acs.bioconjchem.1c00313.

45. Moon, J.; Byun, J.; Kim, H.; Jeong, J.; Lim, E.K.; Jung, J.; Cho, S.; Cho, W.K.; Kang, T. Surface-independent and oriented immobilization of antibody via one-step polydopamine/protein G coating: Application to influenza virus immunoassay. *Macromol. Biosci.* **2019**, *19*, 1800486, https://doi.org/10.1002/mabi.201800486.

46. Byzova, N.A.; Safenkova, I.V.; Slutskaya, E.S.; Zherdev, A.V.; Dzantiev, B.B. Less is more: A comparison of antibody–gold nanoparticle conjugates of different ratios. *Bioconjug. Chem.* **2017**, *28*, 2737-2746, https://doi.org/10.1021/acs.bioconjchem.7b00489.

47. Zvereva, E.A., Byzova, N.A., Sveshnikov, P.G., Zherdev, A.V., Dzantiev, B.B. Cut-off on demand: Adjustment of the threshold level of an immunochromatographic assay for chloramphenicol. *Anal. Methods* **2015**, *7*, 6378-6384, https://doi.org/10.1039/C5AY00835B.